

Article

# Experimental Investigation on Heat Transfer Mechanism of Air-Blast-Spray-Cooling System with a Two-Phase Ejector Loop for Aeronautical Application

Jia-Xin Li <sup>1</sup>, Yun-Ze Li <sup>1,2,3,\*</sup> , Ben-Yuan Cai <sup>1</sup> and En-Hui Li <sup>1</sup>

<sup>1</sup> School of Aeronautic Science and Engineering, Beihang University, Beijing 100191, China;

jxin.lee@buaa.edu.cn (J.-X.L.); caibenyuan@buaa.edu.cn (B.-Y.C.); lienhui@buaa.edu.cn (E.-H.L.)

<sup>2</sup> Institute of Engineering Thermophysics, North China University of Water Resources and Electric Power, Zhengzhou 450045, China

<sup>3</sup> Advanced Research Center of Thermal and New Energy Technologies, Xingtai Polytechnic College, Xingtai 054035, China

\* Correspondence: liyunze@buaa.edu.cn; Tel.: +86-10-8233-8778; Fax: +86-10-8231-5350

Received: 17 September 2019; Accepted: 15 October 2019; Published: 18 October 2019



**Abstract:** This paper presents an air-oriented spray cooling system (SCS) integrated with a two-phase ejector for the thermal management system. Considering its aeronautical application, the spray nozzle in the SCS is an air-blast one. Heat transfer performance (HTP) of air-water spray cooling was studied experimentally on the basis of the ground-based test. Factors including pressure difference between water-inlet-pressure (WIP) and spray cavity one (PDWIC) and the spray volumetric flow rate (SVFR) were investigated and discussed. Under a constant operating condition, the cooling capacity can be promoted by the growth factors of the PDWIC and SVFR with the values from 51.90 kPa to 235.35 kPa and  $3.91 \text{ L} \cdot \text{h}^{-1}$  to  $14.53 \text{ L} \cdot \text{h}^{-1}$ , respectively. Under the same heating power, HTP is proportional to the two dimensionless parameters Reynolds number and Weber number due to the growth of droplet-impacting velocity and droplet size as the increasing of PDWIC or SVFR. Additionally, compared with the factor of the droplet size, the HTP is more sensitive to the variation in the droplet-impacting velocity. Based on the experimental data, an empirical experimental correlation for the prediction of the dimensionless parameter Nusselt number in the non-boiling region with the relative error of only  $\pm 10\%$  was obtained based on the least square method.

**Keywords:** spray cooling; ground-based test setup; two-phase ejector; aeronautical application; empirical experimental correlation

## 1. Introduction

During the last several decades, the electronic components with requirements of miniaturization, highly-integrated and high-density device packaging have applied for a wide variety of industrial and environmental fields. It has developed a dramatic growth in both electrical power and local heat flux. Therefore, thermal management is becoming an increasing need in the development of electronics devices. Especially for aeronautical applications, the heat dissipation requirement would be over an order of  $10^2 \text{ W} \cdot \text{cm}^{-2}$  and the stable operating temperature of airborne electronic equipment should be below  $85 \text{ }^\circ\text{C}$  [1,2]. Therefore, large amounts of waste heat at high heating power must be removed, transported and rejected to an external surrounding using high-efficiency thermal management approaches.

In general, either convective air-cooling or liquid-cooling is the available single-phase method for dissipating waste heat nowadays [3], and the latter option is more attractive due to its high thermal load ability than the former one. However, when a higher level of heat fluxes generated

and face more complicated working conditions such as overload in the aeronautical environment, liquid-cooling techniques often cannot gain sufficient heat dissipation capacity and achieve a relatively stable performance [2,4]. Tremendous studies regarding the heat transfer attainability and discovered that the two-phase convection could afford two- to three-orders-of-magnitude higher heat transfer coefficients over single-phase convection in addition to maintaining closer temperature tolerances [2–6]. Spray cooling is considered as one of the most effective methods of high-flux-waste-heat removal and has long enjoyed a reputation of unavoidable cooling method [7]. It has several remarkable advantages: not only the high heat flux dissipation capacity but also the low-temperature difference with low coolant mass flux in the given condition and its latent heat of vaporization absorbs great amounts of heat with a minimal temperature variation [8,9]. It was reported that its Critical Heat Flux (CHF) could be up to 1200 W/cm<sup>2</sup> when using water as the coolant [6]. Spray phenomenon can be described when working fluid is forced through a nozzle or nozzles array under pressure where the fluid is broken or atomized into numerous tiny droplets. Subsequently, droplets impinge onto a target surface, forming a thin liquid film upon the surface and taking away the waste heat. The effect of droplet-impacting and the thin liquid film in formation are the critical factors that bring about the efficient heat dissipation. The heat transfer mechanism can be summarized in the ways of forced convection, film evaporation, nucleate boiling and second nucleation [10,11].

For the purpose of enhancing the heat dissipation capacity of SCS, tremendous efforts regarding the complicated heat transfer mechanisms have been carried out through both numerical simulation studies and experimental investigations in different conditions. Many parameters affect the thermal performance such as arrangement of multi-nozzle [5], heat transfer surface roughness [6], coolant type [12–14], spray flow rate [13,15–17], spray height [18], spray angle [19], nozzle inlet pressure [20], droplet size [21], impact velocity [22], gravity [4,23], target surface structure [24–27], and sub-cooling degree [28,29], which all have been contributed to the variation in behavior of spray cooling technology. Furthermore, each of the factors is mutual interference and restriction [7], for instance, the factors of droplet size, impact velocity, spray angle, even the spray flow rate would change as the variation of the nozzle inlet pressure. Hence, the heat transfer performance would be affected mainly reflects in both the heat transfer coefficient raises and surface temperature declines with the increasing of inlet pressure (4.5 bar~7.5 bar) under the same operating conditions (spray height with 18 mm and nozzle inlet temperature with 10 °C) and several independent heating powers (500 W, 800 W, 1000 W and 1400 W), published by Zhou et al. [20]. The reason was that the spray flow rate increases with the inlet pressure growth causing the enhancement of the atomization effect, which promotes the liquid shock and liquid film disturbance, in addition, the spray cooling performance was enhanced. The investigation conclusion also indicated that both the impact velocity and the spray flow rate increase with the growth of the inlet pressure, while the droplet size decreases. Under the same heat flux, the cooling ability of spray is proportional to the two dimensionless parameters—Reynolds number  $Re$  and Weber number  $We$ , both of which are improved as the growth of inlet pressure. Furthermore, another effect is that with the increasing of the inlet pressure is the evaporation intensity will decrease, and a larger climb rate of heat transfer coefficient is affected by evaporation intensity when a higher heating power appears, thus the target surface temperature becomes higher and the evaporate capacity becomes stronger.

Moreover, nozzle type is one of the most critical components affecting the spray parameters of the atomization quality [7,30–33], especially for the droplet size and impact velocity are proven significantly correlated with the effectiveness of SCS. Apparently, liquid atomization is an important process contributing to obtain the desired performance of the spray quality. Various liquid atomization strategies are applied for that and twin-fluid atomization is one such technique where the gas energy is employed to promote liquid atomization. The air-blast atomization nozzle (ABAN) is the representative example of the twin-fluid atomization method, in which a liquid sheet is blasted with air jets is allowed to mix with the liquid inside the nozzle to form a spray and the kinetic energy of air is employed to assist liquid breakup [34]. According to the mechanism of air-blast breakup, various designs of

ABANs were discussed in a review article [30], and the Sauter Mean Diameter (SMD) of 75  $\mu\text{m}$  of spray droplet size with water at a gas-to-liquid ratio (GLR) of the value of 1.0 was achieved [31]. In addition, the SMD in the 50  $\mu\text{m}$  order of magnitude can be acquired at a GLR of 8 by Feras et al. [32] during the experimental investigations on swirl ABAN. The SMD of ABAN is far less than that of other type nozzles such as cone nozzle which order of SMD is around 250  $\mu\text{m}$  [33]. Nowadays, the ABAN has been widely employed and played an important role in spray cooling technology in many cases of industrial application because of its excellent atomization quality which directly affects the heat transfer performance of SCS [7,34].

To date, either airborne or ground-based experimental investigation devices so far have been set up to study the parameters related to the heat transfer mechanism for acquiring a better spray cooling performance. However, the essential design of each component has been ignored [33]. As is known to all, the aircraft auxiliary power unit (APU), which consists of a small gas-turbine, is a system designed to supply part of electrical and pneumatic of aircraft. The unit is not limited to start the airplane's main aeroengines, but also provides pneumatic such as aircraft pressurizing [35]. Therefore, the high-pressure air is so available [7] that could provide the primary gas-flow for SCS. Another problem is how to dissipate the waste heat from the sprayed droplet should be resolved to ensure the stability of the system. It is known that the thermal management system (TMS) is an important and indispensable system of the aircraft and the typical heat sinks of TMS including ram-air heat sink, fuel heat sink, and skin heat sink [36], which could be used for dissipating the amount of waste heat from both gas-phase and liquid-phase. Nevertheless, the harsh working conditions will seriously decrease both stability and coefficient of the implementation capacity of the whole system, especially in an overload or microgravity environment. Consequently, more considerable attention should be attracted to the recovery method of liquid-gas two-phase as well as the liquid management technique and its aeronautical application in future research. The ejector has been widely used in the refrigeration system [37], solar energy system [38], desalination system [39], etc. Thanks to the characteristics of simple structure, no moving parts, low-maintenance and low-cost [37,40]. It can persistently produce a vacuum region with accelerated flow velocity in the suction chamber, and the flow-absorbing ability causes by the pressure difference (PD) between the suction chamber and the inlet of second flow. Therefore, the ejector can be employed in SCS of aeronautical applications for the purpose of collecting the liquid-vapor two-phase mixture flow from relatively high pressure in the spray chamber area under the varied-gravity working condition.

Except for the effect of gravity, the environmental pressure (EP) also is a highlight trait in the aerospace in which the spray parameters may be changed due to the PD between the nozzle inlet pressure and the surrounding one. In addition, the heat transfer could be enhanced because of the flash boiling, bringing about an improved thermal transfer performance when the surrounding pressure is lower than the saturation pressure of the coolant [41]. The heat transfer performance influenced by low EP, which range is 0.2–0.4 MPa, was researched by Liu et al. [42]. They discovered that a lower EP resulted in a longer waiting time to evaporate the coolant and a larger superheat degree to active more nucleation sites. The heat is mainly dissipated by convection during the growth process of a bubble so the amount of the heat dissipation at a lower EP is much less than that at a higher EP. Besides, the surface tension and the viscosity of the spray fluid will be influenced by the decrease of the EP, which will lead to bigger droplets size compared with higher EP.

In our present study, an air-blast-spray-cooling system (ABSCS) for aeronautical application is produced by a novel designed with a key two-phase ejector loop using an ABAN. Thermal experiments were organized by the ground-based ABSCS set-up to investigate influences of the PD between water-inlet-pressure (WIP) and spray cavity one (PDWIPSC) as well as SVFR on the heat transfer mechanisms of spray cooling technology. In addition, capable of providing performance predictions and guidance for future full-scaled experiments, further data process and experimental dimensionless study have been organized on the basis of the least square method.

## 2. Concept Design and Experimental Set-Up of ABSCS for Aeronautical Application

### 2.1. Mechanism of the Onboard ABSCS

Figure 1a displays the concept design of the onboard ABSCS. The high pressure and high-temperature air from the APU are first cooled down through the pre-cooling device, then the high pressure and low-temperature air is dispersed into two ways with a three-way valve. The first one is for conventional uses such as the ECS to control temperature of cockpit. The second is used for the current onboard ABSCS as the primary gas-flow for both the air-blast nozzle and mainstream of the ejector. The high thermal load equipment is cooled by spray droplets, then the liquid-vapor mixture is formed in the spray chamber. The two-phase ejector can draw the two-phase flow drives by PD and transfer that to the liquid-vapor separator which outlet of gas-phase and liquid-phase is connected to the outlet of aircraft's ram air and the inlet of recycling water tank respectively. The gas-phase in separator can be drawn by PD due to the high gas flow rate at the ram air outlet, then exhaust into atmospheric environment outside the aircraft, while the liquid-phase flows through the airborne heat exchanger (HX) which is composed of the fuel HX and the skin HX in which the waste heat is respectively transferred into fuel tank and dissipated into external surrounding of the aircraft. The water from skin HX and fuel HX will mix and then deliver back to the recycling water tank in order to spray again.

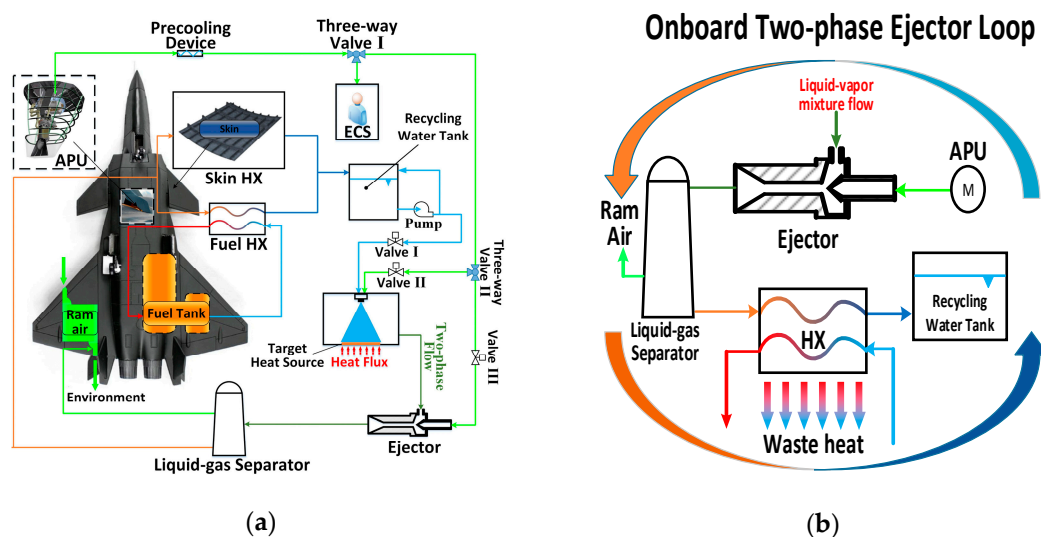


**Figure 1.** Concept design of the proposed onboard ABSCS, (a) Schematic view and (b) Description of the onboard two-phase ejector loop.

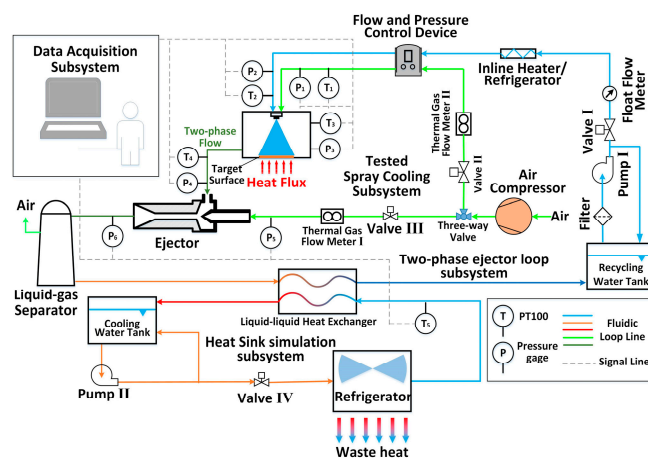
For the aeronautical application, the flexible gravity is a factor worth considering in the spray cooling technology and the most important problem is to discover a method to extract the liquid-vapor mixture formed in the spray chamber. A gas/vapor-liquid two-phase ejector is employed to compose an ejector loop applying to the spray cooling technology which is to solve the difficulty faced in the aeronautical application. The detailed construction of the two-phase ejector loop is shown in the Figure 1b and the working process can be described as follows: the high-pressure air from APU of the airplane flows into ejector's motive nozzle firstly where the velocity of motive flow increases and pressure decreases due to the principle of energy conservation. Hence, the liquid-vapor mixture will be sucked in the ejector's suction nozzle by the PD between spray chamber and ejector's inside. The two branches of flow conflate in the diffuser of the ejector with supersonic speed. Therefore, normal shock develops at the end of the diffuser where the pressure increases and velocity decrease to subsonic level. Accordingly, the pressure of the mixture is further facilitated at the cost of velocity decreasing after discharging from the diffuser which is connected to the airborne HX in which the waste heat dissipated

from the target heat source is extracted to the heat sink. The cooled water runs into the recycling water tank in preparation for reusing back to spray.

## 2.2. Ground-Based ABSCS

### 2.2.1. Experimental Set-Up

For the purpose of studying the heat transfer mechanism of the spray cooling technology and the performance of the focused loop conveniently, a ground-based experimental setup was designed and built up. Figure 2a demonstrates the schematic view of the system and several photographic views of representative system apparatuses. There are three major structural differences between the onboard system and ground-based experimental one: (1) the onboard APU is replaced by an air compressor to provide the high-pressure air for the ABAN and the ejector, (2) the waste heat is dissipated by a heat sink simulation subsystem (HSSS) consists of the liquid-liquid HX, refrigerator and a cooling water tank instead of the onboard HX system, (3) a data acquisition subsystem (DAS) is used to monitor, capture and record all the experimental information. Therefore, the ground-based experimental setup was composed of four parts which were the tested spray cooling subsystem (TSCS), two-phase ejector loop subsystem (TELS), HSSS and DAS. The functionalities of the first three parts were to verify the heat dissipated capacity of the proposed system and the last one was used to collect data. The components of the system including spray chamber, air compressor, two-phase ejector, liquid-gas separator, liquid-liquid HX, recycling water tank, cooling water tank, filter, pumps (2 of), valves (4 of), three-way valve, thermal gas flow meters (2 of), float flow meter, inline heater/refrigerator, flow and pressure control device (FPCD), refrigerator, ABAN, simulated heat source, PT100s (5 of), pressure gages (6 of) and pipelines. The spray chamber attended as a heat collection unit which consists of the nozzle, target surface, and pressure gage. Pipelines were composed of vapor pipes, liquid pipes, and two-phase pipes. The pressure gauges and thermal resistances (PT100s) were used for acquiring several critical pressure and temperature data respectively. Uncertainty analysis of the measurements are shown in the Appendix A.



(a)



(b)

Figure 2. Cont.

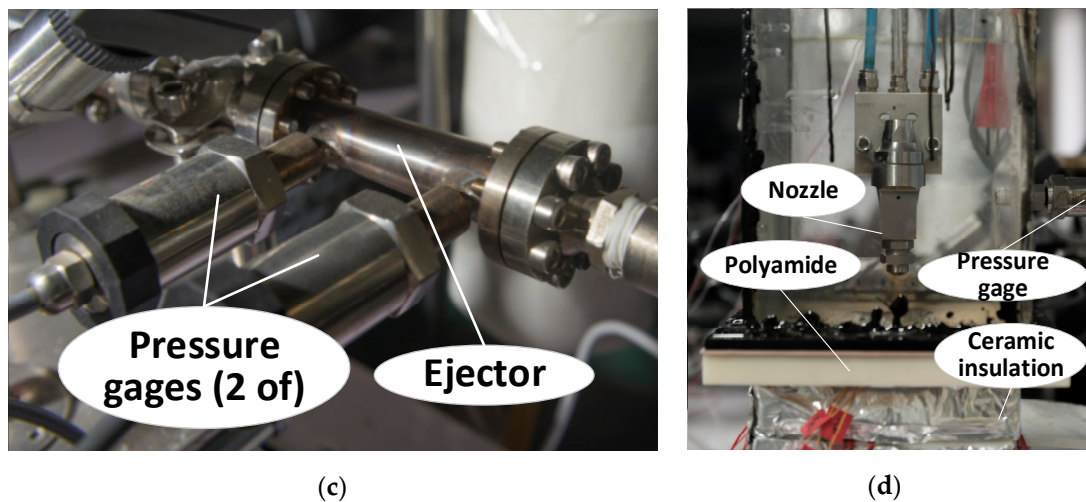


**Figure 2.** The ground-based experimental setup: (a) schematic view of the system, (b) spray control device, (c) two-phase ejector, and (d) spray chamber.

The operation mechanism of the entire ground-based test is described as follows: before entering the nozzle, the ultrapure water in the recycling water tank will be transported through the filter, pump, float flow meter, inline heater/refrigerator, and FPCD to remove the impurities and gain the preferred pressure, experimental desired SVFR and the required sub-cooling. The air compressor is started to provide high-pressure air for both nozzle and ejector. Air-inlet-pressure (AIP) and WIP will be controlled by the FPCD, owing to impact of air-blast depressurization, water is atomized into numerous tiny droplets when passing through the ABAN which is spread out in the chamber and impinged on the target surface removing the waste heat through droplet impact, liquid convection, evaporation, boiling [8], etc. Liquid and vapor mixture then form into the two-phase flow in the spray chamber will be sucked by the upstream of the ejector by the PD. Vapor and liquid, which are merged in the two-phase ejector, are delivered to the liquid-gas separator where the gas is exhausted while the liquid-phase is conveyed to the liquid-liquid HX in which the obtained waste heat is transferred to the HSSS and ultimately discarded to the external surroundings by the refrigerator.

### 2.2.2. ABAN in Spray Chamber

Droplet size distribution is a considerable parameter of the atomization process besides droplet mean diameter. The smaller atomized droplet size can promote the waste heat dissipation capacity during the spray cooling process [21]. ABAN has been widely used and played a crucial role in the high-heat-flux dissipation field of industrial application because the atomized droplets size is smaller than that of other types of nozzles. In the present study, an ABAN, which type is 1/4J Set-Up Air Atomizing Nozzle made by Spraying Systems Co. from America, was utilized to investigate the heat transfer performance of spray cooling technology. The ABAN has three inlets including one liquid inlet and two gas inlets which are air-pressure inlet and air-control inlet respectively, the latter air inlet is used to control opening and closing of the nozzle. Figure 3 shows the photographic view of the practical nozzle. Ultrapure water and air were employed as the experimental liquid and gas respectively in the present study. Photographic views of spray angle with different pressure differences between WIP and spray cavity one (PDWICs) are shown in Figure 4 and SMD for various WIP and AIP are plotted in Figure 5. Especially, the value of AIP was 249.92 kPa had been employed in the current study and whose fundamental hydrodynamic properties are provided in Table 1. Data was based on spraying water under laboratory conditions and all values were to be computed utilizing the procedures for determining spray characteristics as outlined by American Society of Testing Materials (ASTM) (Standard E799).



Figure 3. Photographic view of the practical 1/4J Set-Up Air Atomizing Nozzle.

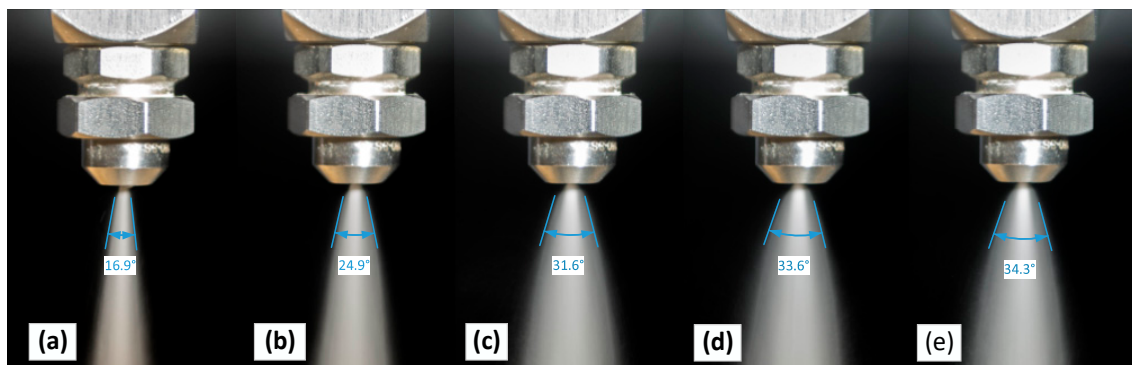


Figure 4. Photographic views of spray angle with PDWIC, (a)  $P_{diff} = 51.90$  kPa, (b)  $P_{diff} = 93.73$  kPa, (c)  $P_{diff} = 145.85$  kPa, (d)  $P_{diff} = 201.61$  kPa, and (e)  $P_{diff} = 235.35$  kPa.

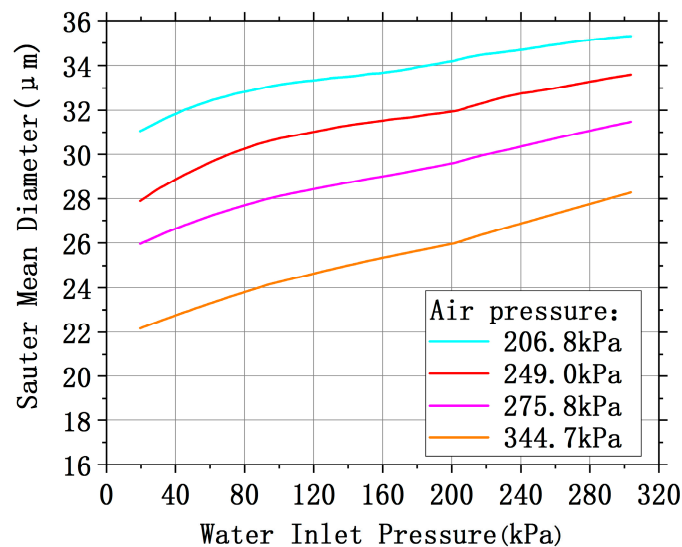


Figure 5. Sauter Mean Diameter (SMD) for water-inlet-pressure (WIP) and Air-inlet-pressure (AIP).

Table 1. Fundamental hydrodynamic properties of the nozzle employed in the current study.

Orifice Diameter (mm)	Spray Angle ( $^{\circ}$ )	Sauter Mean Diameter ( $\mu\text{m}$ )	Spray Volumetric Flow Rate ( $\text{L}\cdot\text{h}^{-1}$ )
1.1	16.9–4.3	22.1–35.4	3.91–14.53

As a result, the nozzle is locked in the spray chamber as shown in Figure 2d, which is the central part of the current experimental closed fluidic loop. Multiple tasks are undertaken in the spray chamber including spray, heat exchange, self-sustained fluidic pumping, air-water separation, air/water transportation, and water collection. The bottom of the spray chamber is made of polyamide with a drilled cubical hole to embed the head of the simulated heat source. A drainage hole connecting

a tube is also drilled in the bottom which is arranged for drawing the sprayed water and air and draining them out into the two-phase pipe linking to the ejector. The other five sides are made of transparent acrylic material for easy visual observation and photographs. The top side of the chamber has three threaded holes through which three 304 stainless steel tubes connecting three inlets of the ABAN. A thermal resistor and a pressure sensor probe are secured in the vertical internal wall of the chamber for the purpose of temperature measurement and pressure measurement of the surrounding vapor in the spray chamber.

### 2.2.3. Simulated Heat Source

Figure 6 shows the constructional details of the simulated heat source which is to simulate the high-heat-flux generation and heat exchange process. The simulated heat source is made of oxygen-free copper with a cylindrical body which is surrounded by thermally insulated ceramic materials to reduce the heat loss. Table 2 lists the thermophysical parameters of the copper. In order to ensure the heat source's target surface is exposed to be sprayed, the cubical head locked in a fiberglass insulation board, which is used to reduce the heat loss, is inserted into the bottom of the spray chamber which is made of polyamide. The high-temperature-resistant grease is used to help the cubical head to be placed tightly against the hole which is drilled in the spray chamber's bottom and guaranteed the fixation of the heat source assembly and no leakage of the excess sprayed liquid permeating through the bottom and inside the heat source. The simulated heat flux is produced by 120 W cartridge electric heaters (13 of) which are embedded into simulated heat source's underside and connected parallel to a contrivable power supply. Six sheathed 2 mm-diameter type-K thermocouples are locked into two bedding layers (3 of) at distances of  $l_{s-up}$  and  $l_{s-low}$  from the target surface to monitor those planes' temperatures which are represented by  $\bar{T}_{up}$  ( $T_{up1}$ ,  $T_{up2}$ , and  $T_{up3}$ ) and  $\bar{T}_{low}$  ( $T_{low1}$ ,  $T_{low2}$ , and  $T_{low3}$ ) respectively. The data can be used to conclude the heat flux, temperature and heat transfer coefficient of the target surface during the experiments based on the Equations (1)–(4).

$$\bar{T}_{up} = \frac{\sum_{i=1}^3 T_{upi}}{3}, \quad \bar{T}_{low} = \frac{\sum_{i=1}^3 T_{lowi}}{3} \quad (1)$$

$$q = \lambda_{cu} \cdot \frac{\bar{T}_{low} - \bar{T}_{up}}{l_{s-low} - l_{s-up}} \quad (2)$$

$$T_{sur} = \bar{T}_{up} - \frac{q l_{s-up}}{\lambda_{cu}} = \bar{T}_{low} - \frac{q l_{s-low}}{\lambda_{cu}} \quad (3)$$

$$h = \frac{q}{T_{sur} - T_{in}} \quad (4)$$

Since the focus in this paper is to constitute a test heater that can simulate the heat generation capability of the aeronautical on-board application, a smooth surface area of  $12 \times 12 \text{ mm}^2$  for dissipating waste heat was used in the current study considering only one ABAN was utilized in the spray chamber as well. As a result, through the total actual heat of practical aeronautical application would not be accomplished by the simulated heat source, the heat generation capability in terms of heat flux could be realized. Figure 6a displays the photographic and cross-sectional view of the smooth surface on the oxygen-free copper block.

**Table 2.** Thermophysical parameters of copper.

Temperature (°C)	Thermal Diffusivity ( $\text{m}^2 \cdot \text{s}^{-1}$ )	Specific Heat at Constant Pressure ( $\text{J} \cdot \text{kg}^{-1} \cdot \text{K}^{-1}$ )	Density ( $\text{kg} \cdot \text{m}^{-3}$ )	Thermal Conductivity ( $\text{W} \cdot \text{m}^{-1} \cdot \text{K}^{-1}$ )
25	$6.42 \times 10^{-5}$	470.8632	$8.945 \times 10^3$	270.55
100	$6.73 \times 10^{-5}$	480.8412	$8.945 \times 10^3$	289.50

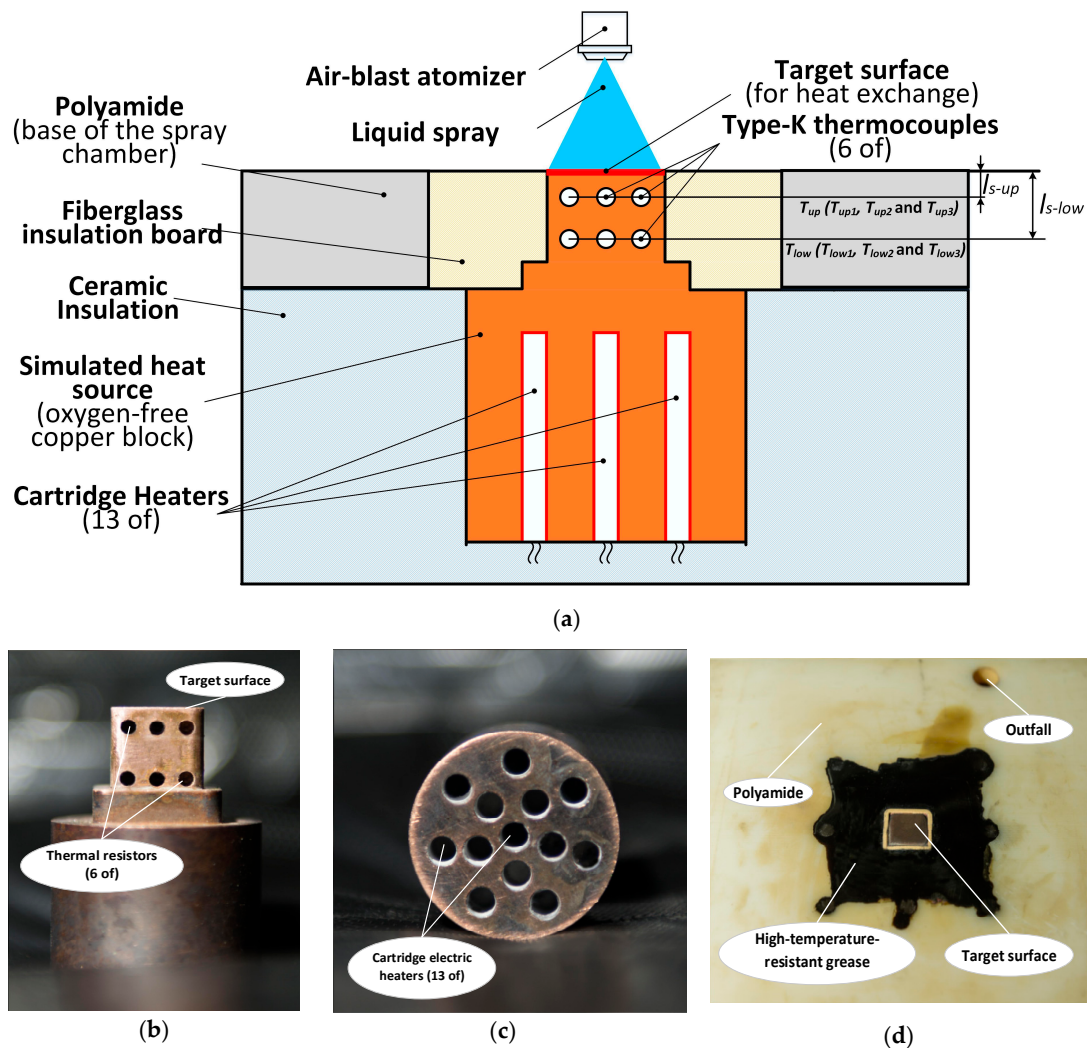


**Figure 6.** The simulated heat source and several photographic views: (a) the constructional details of it, (b) frontal view, (c) bottom view, and (d) cross-sectional view of the smooth surface.

### 2.3. Operating Condition Arrangement and Experimental Procedure

The purpose of the current investigation is to study the influences of PDWICs and spray flow rate on the spray cooling heat transfer performance, whose related experimental operation conditions are listed in Table 3. Transparently, the cases 1–5 were arranged to research the effects of various PDWICs on spray cooling performance, while cases 6–10 to examine the impacts of various spray volumetric flow rates (SVFRs) on the heat transfer mechanism. Note that the ABAN was employed during all the scheduled tests. All experiments were conducted with the same AIP and constant water inlet temperature of 249.92 kPa and 22.92 °C respectively, and an invariable spray distance of 60 mm was fixed ensuring that the spray impact area was well covered upon the target surface.

Prior to the experiment, all test components must be connected to completion. Especially, the simulated heat source should be prudently embedded in the bottom making sure that no leakage of the excess sprayed liquid permeating through the bottom and inside the heat source, and the nozzle was placed right above the target surface. Tests were initiated by prudently sealed the spray chamber and connected all the electric wire and data bus well. Ultrapure water was filled into the recycling water tank and power was inputted into the preheater in order to obtain preferred liquid temperature. Note that all the present tests were structured under the constant operation of the two-phase ejector loop.

**Table 3.** Description of experimental operation conditions.

Case	Various Parameters Description	
	Pressure Difference between Water Inlet Pressure and the Cavity One (kPa)	Spray Volumetric Flow Rate (L·h <sup>-1</sup> )
1	51.90	9.08
2	93.73	9.08
3	145.85	9.08
4	201.61	9.08
5	235.35	9.08
6	145.85	3.91
7	145.85	4.97
8	145.85	9.08
9	145.85	13.66
10	145.85	14.53

The first test group conducted cases 1–5, which was to study the effect of the PDWIC and the formal preparation of the heat transfer performance investigation experiments upon spray cooling technology. The tests were organized subject to the following procedures: (1) activate the data acquisition subsystem preparing for data collection and record during each run, (2) initialize the pump II to operate the water-cooled device, (3) in order to ensure no water flood in the spray chamber when spray begins, the ejector should be operated by initialized the air compressor, (4) activate the pump I starting the beginning of the spray system, (5) the SVFR and water temperature at nozzle inlet can be regulated by the adjustment of pump speed and inline heater/refrigerator respectively, (6) adjust spray system to regulate AIP and PDWIC to the values of 249.92 kPa and 51.90 kPa respectively for at least 5 min allowing the liquid to circulate through the whole loop and ensuring flow stability of the spray, (7) regulate each cartridge electric heater (10 of) for the input voltage to 4 V heating the copper block at first, waiting the entire simulated heat source to acquire the stable temperature for at least 10 min and storing the collected data, (8) after gaining stabilization, increase the input voltage to 8 V, 12 V, 16 V, 20 V, 24 V, and 28 V, then repeat the step (7) and (8), (9) gradually drop the input voltage to 0 V and cool down the entire simulated heat source to original state, regulate the PDWICs to the value of 93.73 kPa, 145.85 kPa, 201.61 kPa and 235.35 kPa and keep the AIP constant, then repeat the steps (6)–(9).

The second test group was to go on cases 6–10, which main steps of formal experiments were similar to the first group's, investigated the influence of cooling ability as the various SVFRs which was controlled by the pump I and monitored by the float flow meter.

### 3. Experimental Results and Discussions

Experiments were focused on the investigation of the basic heat transfer performance of the two-phase ejector assisted SCS with an ABAN, exploring its capability of dissipating waste heat for aeronautical applications. Effects of PDWIC and SVFR upon the performance of spray cooling including target surface temperature and heat transfer coefficient with different heat fluxes were examined. According to the results of test measurement, it is suitable for dimensionless analysis study of the spray cooling performance.

#### 3.1. Effects of PDWIC

Experiments were focused on the investigation of the basic heat transfer performance of the two-phase ejector-assisted SCS with an ABAN, exploring its capability of dissipating waste heat for aeronautical applications. Effects of PDWIC and SVFR upon the performance of spray cooling including target surface temperature and heat transfer coefficient with different heat fluxes were examined. According to the results of test measurement, it is suitable for dimensionless analysis study of the spray cooling performance.

Experimental data of cases 1–5 with different heating powers are displayed in Figure 7. The PDWICs were adjusted from 51.90 kPa to 235.35 kPa and the heat fluxes increased by 5 levels ( $32.18 \text{ W} \cdot \text{cm}^{-2}$ ,  $63.19 \text{ W} \cdot \text{cm}^{-2}$ ,  $100.37 \text{ W} \cdot \text{cm}^{-2}$ ,  $181.34 \text{ W} \cdot \text{cm}^{-2}$ , and  $222.73 \text{ W} \cdot \text{cm}^{-2}$ ), and the test data was attained under the steady-state condition. Characteristic curves of the heat transfer coefficient as a function of PDWIC and surface temperature as a function of PDWIC are shown in Figure 7a,b respectively.

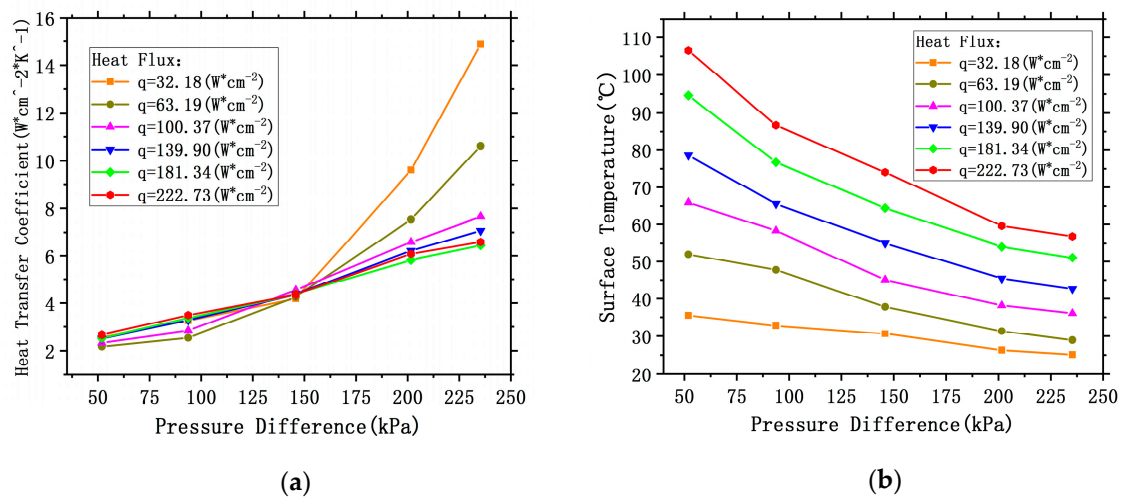


**Figure 7.** Characteristic heat transfer curves for various heat fluxes, (a) heat transfer coefficient as a function of spray cavity one (PDWIC) and (b) surface temperature as a function of PDWIC.

As shown in Figure 7, it can be obviously observed from the pattern (a) that the heat transfer coefficient displays an upward tendency with different slopes as the PDWIC increases because of the droplet-enlarging dissipate more waste heat [20]. Besides, the heat transfer coefficient under a smaller heating power increases faster than that under a larger heating power. Combining with pattern (b), it is obvious that the temperature under a smaller heat flux is lower than that under a larger heat flux, indicating that the target surface temperature is closer to the water inlet temperature, due to the calculated mode of the heat transfer coefficient Equation (4). The heat transfer coefficient is inversely proportional to the temperature difference between the target surface temperature and the water inlet one. Therefore, the heat transfer coefficient will be larger under lower heat fluxes than that under higher heat fluxes when the value of the temperature difference is enough small. Clearly observed from pattern (a) that all characteristic curves separate into two stages at the pressure difference of 145.85 kPa. In the formal stage, the heat transfer coefficient climbs with the small slope as the PDWIC increases, and the value of heat transfer coefficient under a higher heat flux is bigger than that under a low heat flux. While in the latter stage, when PD exceeds 145.85 kPa, the slope of characteristic curves increases dramatically especially for the condition under the lowest heat flux ( $32.18 \text{ W} \cdot \text{cm}^{-2}$ ) which is depicted by an orange curve in Figure 7a. The heat transfer coefficients at this PD point are all around  $4.2 \text{ W} \cdot \text{cm}^{-2} \cdot \text{K}^{-1}$ , so it could be concluded that this value is a turning point dividing the spray cooling to two different stages as previous statement.

Pattern (b) shown in Figure 7 is demonstrated the characteristic relation between target surface temperature and the PDWIC. A similar decreasing tendency of the target temperature is displayed as the dilation of PD. In addition, the slope is weakened as the PD increases because the target temperature is more approach to the water inlet temperature.

Larger PDWIC indicates larger WIP and higher initial velocity of each spray droplet, meaning that the waste heat dissipated by droplet-impacting will be promoted. However, the SMD become larger as the WIP increasing when the AIP under a constant condition, which is demonstrated in Figure 5. As a result, both the two dimensionless parameters Reynolds number  $Re$  and Weber number  $We$ , which are calculated by Equation (5) [42] and (6) [18] respectively, are increased with the growth of

WIP. Under the same heating power, the heat dissipation capacity of spray cooling is proportional to  $Re$  and  $We$ .

$$Re = \frac{\rho u_{dro} d_{32}}{\mu} \quad (5)$$

$$We = \frac{\rho u_{dro}^2 d_{32}}{\sigma} \quad (6)$$

Table 4 organizes the comparisons of thermal parameters (temperature and heat transfer coefficient) for cases 1 to 5. Under a lower heat flux ( $32.18 \text{ W} \cdot \text{cm}^{-2}$ ), with the PDWIC increases from 51.90 kPa to 235.35 kPa, temperature reduction is  $-29.28\%$ , which is smaller than that under a larger heat flux (when heat flux is  $222.73 \text{ W} \cdot \text{cm}^{-2}$ , temperature reduction is  $-46.75\%$ ). However, the heat transfer coefficient enhancement has an opposite trend compares to that of temperature reduction. With the same growth of the PDWIC, the heat transfer coefficient enhancement is 480.86% when the heat flux is  $32.18 \text{ W} \cdot \text{cm}^{-2}$ , while the heat transfer coefficient enhancement is only 147.43% under a high heat flux of  $222.73 \text{ W} \cdot \text{cm}^{-2}$ .

**Table 4.** Comparisons of the thermal parameters.

Heat Flux ( $\text{W} \cdot \text{cm}^{-2}$ )	PDWIC (kPa)	Temperature ( $^{\circ}\text{C}$ )	Temperature Reduction	Heat Transfer Coefficient ( $\text{W} \cdot \text{cm}^{-2} \cdot \text{K}$ )	Heat Transfer Coefficient Enhancement
32.18	51.90	35.49	/	2.56	/
	235.35	25.10	$-29.28\%$	14.87	480.86%
63.19	51.90	52.00	/	2.17	/
	235.35	28.89	$-44.44\%$	10.62	388.35%
100.37	51.90	65.94	/	2.33	/
	235.35	36.04	$-45.34\%$	7.66	228.34%
139.90	51.90	78.61	/	2.51	/
	235.35	42.72	$-45.66\%$	7.07	181.41%
181.34	51.90	94.61	/	2.53	/
	235.35	51.07	$-46.02\%$	6.45	154.76%
222.73	51.90	106.52	/	2.66	/
	235.35	56.72	$-46.75\%$	6.59	147.43%

In general, a better spray cooling performance can be acquired by increasing the velocity of droplet-impacting [20] and decreasing the SMD of spray droplet size [19]. However, according to the analysis of the current experimental investigation, the target surface temperature decreases as the velocity of droplet-impacting increases and the SMD of spray drop size, so it could be drawn a conclusion that the spray cooling performance, which can be promoted by increasing the PDWIC, is more sensitive to the variation in the droplet-impacting velocity compared with the factor of the droplet size.

### 3.2. Effects of SVFR

Characteristic curves of thermal traits plotted in the form of heat flux versus heat transfer coefficient and heat flux versus surface temperature for various SVFRs of case 6–10 ranging from  $3.91 \text{ L} \cdot \text{h}^{-1}$  to  $14.53 \text{ L} \cdot \text{h}^{-1}$  are demonstrated in Figure 8a,b respectively. Experiments in this group were conducted with the same AIP, constant water inlet temperature and invariable spray height of 249.92 kPa,  $22.92 \text{ }^{\circ}\text{C}$  and 60 mm respectively, especially a fixed PDWIC with a middle value (145.85 kPa) of case 1–5 was applied for testing. The experimental heat fluxes were various values ranging from  $30 \text{ W} \cdot \text{cm}^{-2}$  to  $230 \text{ W} \cdot \text{cm}^{-2}$ .

According to Figure 8, it can be clearly observed from pattern (a) that models of heat transfer for each case experience two stages under a lower SVFR ( $\leq 13.66 \text{ L} \cdot \text{h}^{-1}$ ). Stage one, under a lower heat flux ( $< 65 \text{ W} \cdot \text{cm}^{-2}$ ), the slope of each curve is small and the heat transfer coefficient reduces linearly, when the SVFR reaches the level of  $13.66 \text{ L} \cdot \text{h}^{-1}$  (case 9), reduction point of heat flux is up to the value of  $181 \text{ W} \cdot \text{cm}^{-2}$ . In the other stage, curves of the heat transfer coefficient show an upward trend

with a small slope when heat fluxes are larger than  $65 \text{ W} \cdot \text{cm}^{-2}$  and  $181 \text{ W} \cdot \text{cm}^{-2}$  for the first three cases (cases 6–8) and case 9 respectively. While the entire curve of case 10 from pattern (a) displays a decreasing tendency due to its SVFR is larger than the former cases (case 6–9), and the heat transfer coefficient of its characteristic curve has a distinct variation could be obvious noticed. Experimental data is processed into curves of the surface temperature as a function of heat flux demonstrated in pattern (b), overall which showing an upward tendency means that the target surface temperature rises by the increasing heat flux. Under the invariable heating condition, the temperature under a lower SVFR is higher than that under a larger SVFR. It easily took stock of the difference of slope between each case indicating that the spray cooling capability is becoming greater with the SVFR growing up. The temperature differences between each case have no obvious gap under a low heat flux, while under a higher heating condition, the temperature differences will increase. Therefore, the effectiveness of spray cooling with a higher SVFR has better performance under high heat fluxes.

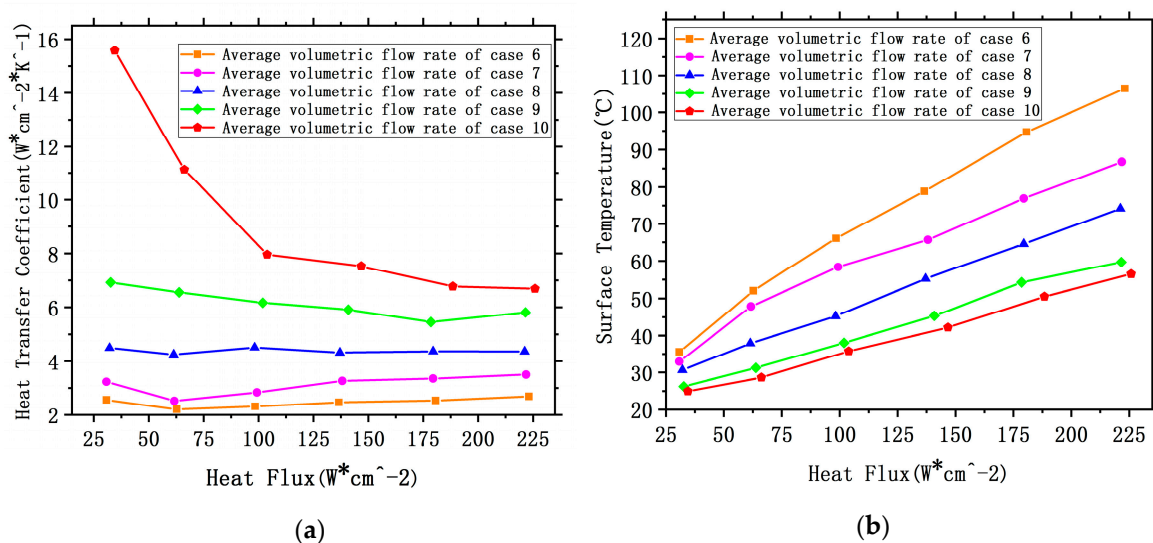


**Figure 8.** Characteristic heat transfer curves for various spray volumetric flow rates (SVFRs), (a) heat transfer coefficient as a function of heat flux and (b) surface temperature as a function of heat flux.

In the first stage, combine the two patterns as shown in Figure 8a,b to analysis, the target surface temperatures are all below  $55 \text{ }^{\circ}\text{C}$ , the heat transfer form of convection is governed in this region. As a result of Equation (4), the heat transfer coefficient is inversely proportional to the temperature difference between the target surface temperature and the water inlet one, so the heat transfer coefficient will be larger under lower heat fluxes than that under higher heat fluxes when the value of the temperature difference is enough small. Accordingly, the decreasing tendency of the characteristic curve of case 10 is a reasonable conclusion for the heat transfer mechanism. As the heat flux rises and the target surface temperature increases, the heat transfer steps to the second stage, evaporative spray occurs where the heat transfer ability is enhanced. In addition, a thin film is forming on the target surface where the bubble's generation and transportation proceed [31] which accounts for the elevation of the heat transfer coefficient.

Table 5 organizes the comparisons of the thermal parameters (temperature and heat transfer coefficient) for case 6 to 10 under the common maximum heat flux  $221.29 \text{ W} \cdot \text{cm}^{-2}$  with different SVFR. Compared with the SVFR of case 6, the SVFRs of other cases (cases 7–10) have gradually increased. The corresponding temperature reductions are  $-18.03\%$ ,  $-29.72\%$ ,  $-43.58\%$ , and  $-47.59\%$  respectively. Additionally, the heat transfer coefficients have been enhanced by  $30.71\%$ ,  $63.30\%$ ,  $117.23\%$ , and  $145.32\%$  respectively.

**Table 5.** Thermal parameters for case 6–10 at the heat flux of  $221.29 \text{ W}\cdot\text{cm}^{-2}$ .

Case	SVFR ( $\text{L}\cdot\text{h}^{-1}$ )	SVFR Enhancement	Temperature ( $^{\circ}\text{C}$ )	Temperature Reduction	Heat Transfer Coefficient ( $\text{W}\cdot\text{cm}^{-2}\cdot\text{K}$ )	Heat Transfer Coefficient Enhancement
6	3.91	/	105.56	/	2.67	/
7	4.97	27.11%	86.53	−18.03%	3.49	30.71%
8	9.08	132.23%	74.19	−29.72%	4.36	63.30%
9	13.66	249.36%	59.56	−43.58%	5.80	117.23%
10	14.53	271.61%	55.32	−47.59%	6.55	145.32%

Generally speaking, either convective or evaporative heat transfer coefficient of spray cooling application growth as the spray flow rate increases. In the stage of convective cooling, a larger SVFR means a higher initial velocity of each droplet, therefore, the heat-dissipating influence of droplet-impacting will be reinforced. In the stage of evaporative heat transfer, a larger SVFR indicates that more coolants will fall over to the heat exchange surface, which suggests sufficient water to be evaporated and thus more waster heat will be dissipated. It can be concluded that the large spray SVFR can facilitate the decrease in the target surface temperature and gain a higher heat transfer coefficient of spray cooling technology which is beneficial for the operational effectiveness of the high-power electronic equipment for aeronautical application.

### 3.3. Experimental Dimensionless Correlation

It is acknowledged that the current study is focused on the small-scale experimental investigation. Although several heat transfer mechanisms of spray cooling with an ABAN based on the experimental data have been discovered by the results analyses and explanations described above, few quantitative conclusions could be drawn to give guidance for further full-scaled applications. In order to generalize the heat transfer laws of spray cooling deduced from the experimental data and enlighten the future application of the novel cooling technology, further data process, and experimental dimensionless study has been organized. Since the flow diffusion in the current condition where the air is applied, the Knudsen number  $Kn$  [41] is a critical parameter to implement the full-scale application and criteria to choose the correct models to describe the spray flow state as well.  $Kn$  is defined by Equation (7) where  $\kappa$  is the mean free path of the molecule which can be calculated by Equation (8) and the parameter  $D$  is characteristic length of the experimental surface which is equal to value of the equivalent hydraulic diameter. Its value can be calculated by Equation (9) where  $A$  and  $C$  represent the area and perimeter of the surface respectively.

$$Kn = \frac{\kappa}{D} \quad (7)$$

$$\kappa = \frac{3.2\mu}{P_{env}} \left( \frac{RT}{2\pi M} \right)^{1/2} \quad (8)$$

$$D = \frac{4A}{C} \quad (9)$$

The calculation results of the longest mean free path of molecules are to be  $4.36 \times 10^{-7} \text{ m}$  and  $6.57 \times 10^{-8} \text{ m}$  for the water molecule and air molecule respectively under the condition of standard atmospheric pressure. Accordingly, the largest  $Kn$  is calculated to be  $3.36 \times 10^{-5}$  for the water molecule and  $5.06 \times 10^{-6}$  for the air molecule. All the calculation values are smaller than 0.01 indicating that the conclusion of the continuum flow can be engaged in the current study, which promotes the further establishment of suitable mathematical models in describing the air-blast atomization spray cooling phenomenon.

The heat transfer performance of spray cooling technology is influenced by many factors that are classified into various parameters such as SVFR, SMD, pressure (AIP, WIP, and cavity pressure), etc. According to the principle of dimensionless investigation, a set of dimensionless parameters,

which are concluded from all the correlative properties, is summarized in Equation (10). As a result, the dimensionless parameters cannot be drawn a comprehensive induction of spray cooling technology during the current investigation.

$$f(h, D, D_s, G_m, \lambda, \mu, c_p, T_{sur}, T_{in}, T_{sat}, P_{water-in}, P_{cavity}) = 0 \quad (10)$$

The two basic dimensionless numbers of the convective heat transfer, the Reynolds number  $Re$  and the Prandtl number  $Pr$  are also two critical factors of spray cooling technology.  $Re$  indicates the flow condition of the liquid film and  $Pr$  reflects the relative thickness of the hydrodynamic and thermal boundary layers. The influence of the ratio of convective to conductive heat transfer upon the surface is represented by Nusselt number  $Nu$ . Equations (11)–(14) defines  $Re$ ,  $Pr$ , and  $Nu$ , respectively. The parameter  $D_s$  in Equation (11) represents the projection diameter of spray on the heat transfer surface which is described in Figure 9 and calculated by Equation (14).

$$Re = \frac{G_m D_s}{\mu} \quad (11)$$

$$Pr = \frac{c_p \mu}{\lambda} \quad (12)$$

$$Nu = \frac{hD}{\lambda} \quad (13)$$

$$D_s = 2H \tan\left(\frac{\alpha}{2}\right) \quad (14)$$

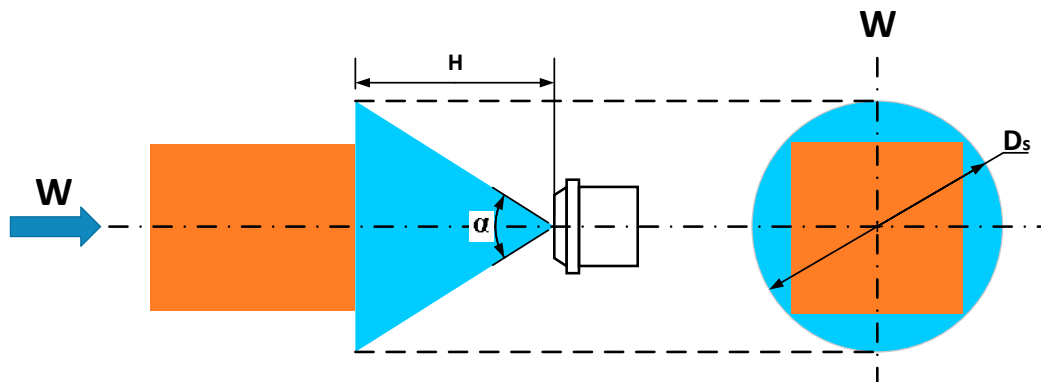


Figure 9. Schematic and simplified version of projection diameter.

Evaporation intensity is acquired by dimensionless temperature  $T^*$  which is defined by Equation (15). Dimensionless pressure  $P^*$ , which is also a vital factor related to the heat transfer performance of spray cooling technology, is calculated by Equation (16).

$$T^* = \frac{T_{sur} - T_{water-in}}{T_{sat}} \quad (15)$$

$$P^* = \frac{P_{water-in} - P_{cavity}}{P_{air-in}} \quad (16)$$

The Equation (17) can be achieved from the manipulation of Equation (10) based on the analysis. Selecting the dimensionless number  $Nu$  as the dependent variable and other parameters as the independent ones, the fitting experimental empirical correlation can be considered to a Nusselt number prediction equation which is especially described by Equation (18). Since all experimental condition is below the saturation temperature, so the test data only in the no boiling heat transfer region is further processed and studied in this dimensionless investigation section.

$$F(Nu, Re, Pr, T^*, P^*) = 0 \quad (17)$$

$$Nu = zRe^{z_1}Pr^{z_2}T^{*z_3}P^{*z_4} \quad (18)$$

In Equation (18),  $z$ ,  $z_1$ ,  $z_2$ ,  $z_3$ , and  $z_4$  are the fitting coefficients which are attained applying for the least square method based on the calculated parameters under the experimental cases in the current study. The final fitting experimental empirical correlation is described by Equation (19) which discloses all the coefficients. The applicable conditions of correlation are (61.2459, 474.4897) for  $Re$ , (2.7805, 6.5201) for  $Pr$ , (0.0218, 0.8360) for  $T^*$ , and (0.2077, 0.9417) for  $P^*$ . The R-Square and the Chi-Square tolerance values of 0.9766 and  $1 \times 10^{-10}$  are reached respectively. Comparisons between the experimental  $Nu$ s and predicted ones based on Equation (A4) are plotted in Figure 10, which shows the test data are predicted within the error bond of  $\pm 10\%$ . According to the error analysis, an ideal prediction for air-blast spray cooling performance not limited in the operating conditions uncovered in this study could be given by the fitting experimental empirical correlation, acquiring relatively high generalizability and direction for later full-scale application.

$$Nu = 0.1790Re^{0.2555}Pr^{-1.8466}T^{*-0.1569}P^{*0.3238} \quad (19)$$

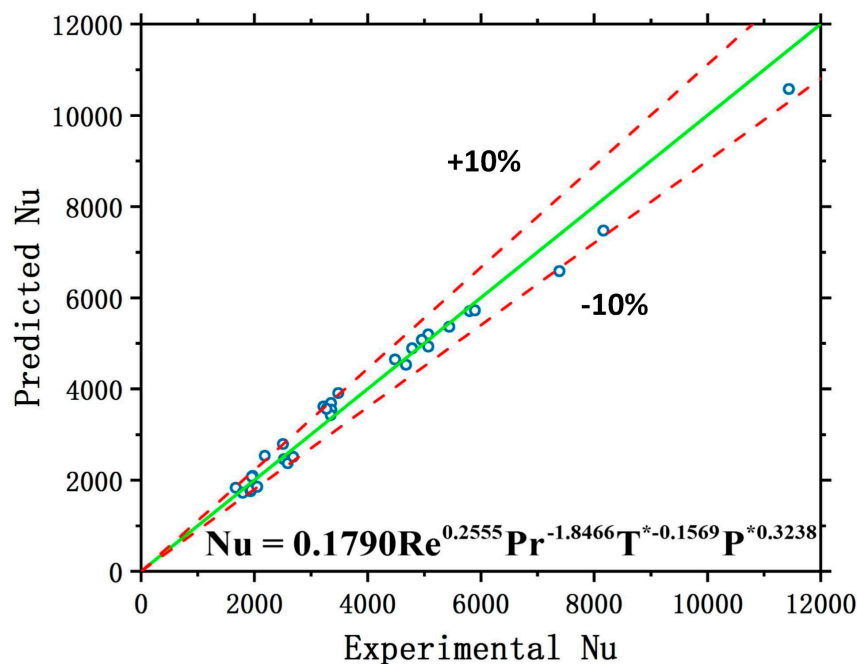


Figure 10. Comparison between experimental  $Nu$  and the predicted ones.

#### 4. Conclusions and Future

Waste heat dissipation in the aeronautical application has become a troublesome problem since the increase in both electrical power and local heat flux are demanded in this field. For the purpose of solving the issue, a novel ground-based ABSCS integrated with a two-phase ejector using an air-blast atomization nozzle (ABAN) was developed to investigate the heat transfer mechanism so as to enhance the cooling capacity. Techniques of the liquid management and vapor-liquid mixture collection in aerospace were introduced as well. Thorough experiments were carried out employing ultrapure water with variation pressure difference between water-inlet-pressure and spray cavity one (PDWIC) and spray volumetric flow rate (SVFR) from 51.90 kPa to 235.35 kPa and  $3.91 \text{ L} \cdot \text{h}^{-1}$  to  $14.53 \text{ L} \cdot \text{h}^{-1}$

respectively. It examined the influences of PDWIC and SVFR upon the heat transfer performance. The following are the primary conclusions:

- Both PDWIC and SVFR are critical factors affecting the heat transfer performance of ABSCS. Under a constant operating condition, the cooling capacity can be promoted by a greater PDWIC or a higher SVFR respectively.
- Under the same heating power, the heat dissipation capacity of spray cooling is proportional to the two dimensionless parameters Reynolds number  $Re$  and Weber number  $We$  due to the variation of droplet-impacting velocity and droplet size as the change of PDWIC or SVFR.
- Compared with the factor of the droplet size, the spray cooling performance is more sensitive to the variation in the droplet-impacting velocity.

Besides, taking almost all the test parameters into account and carrying out-execute organize the experimental dimensionless study, an empirical experimental correlation for dimensionless number of Nusselt number  $Nu$  prediction was obtained on the strength of test feedback attained in non-boiling region which was the center in the current research. The developed calculator can provide good divination for generalizing the heat transfer laws of spray cooling deduced from the experimental data and enlightening the future application of the novel cooling technology with the relative error of only  $\pm 10\%$ . Additionally, the influences of enhanced surface structure, spray height, coolant type will be the central focuses in our future investigations.

**Author Contributions:** Conceptualization, Y.-Z.L.; methodology, J.-X.L.; formal analysis, J.-X.L.; writing—original draft preparation, J.-X.L. and B.-Y.C.; writing—review and editing, E.-H.L.

**Funding:** The project was funded by the Open Research Fund of Key Laboratory of Space Utilization, Chinese Academy of Sciences through grant no. LSU-JCJS-2017-1.

**Acknowledgments:** The work uncovered in the present paper was conducted at the Spacecraft Thermal Control Laboratory, Beihang University.

**Conflicts of Interest:** The authors declare no conflict of interest.

## Nomenclature

$T$	Temperature ( $^{\circ}\text{C}$ )	low	location of low
$\bar{T}$	Average temperature ( $^{\circ}\text{C}$ )	i	location of i (i = 1, 2, 3)
$T^*$	Dimensionless temperature	sur	target surface
q	Heat flux ( $\text{W}\cdot\text{cm}^{-2}$ )	in	inlet
$l$	Length (m)	env	environment
$u$	Velocity ( $\text{m}\cdot\text{s}^{-1}$ )	sat	Saturation condition
$P$	Pressure (Pa)	cu	oxygen-free copper block
$P^*$	Dimensionless of pressure	s-up	Target surface—location up
h	Heat transfer coefficient ( $\text{W}\cdot\text{m}^{-2}\cdot\text{K}^{-1}$ )	s-low	Target surface—location low
$d$	Diameter (m)	dro	droplet
$d_{32}$	Sauter mean diameter (c)	water-in	Water inlet
D	characteristic length (m)	air-in	Air inlet
$D_s$	Projection diameter of spray on the target surface (m)	cavity	Spray cavity
A	Area ( $\text{m}^2$ )	diff	Pressure difference
C	Perimeter (m)	y	Parameter substitution symbol
R	Gas constant ( $8314 \text{ N}\cdot\text{m}\cdot\text{kmol}^{-1}\cdot\text{K}^{-1}$ )	Acronyms	
M	Molar mass (g/mol)	SCS	Spray Cooling System
H	Height (m)	HTP	Heat Transfer Performance
$c_p$	Specific heat at constant pressure ( $\text{J}\cdot\text{kg}^{-1}\cdot\text{K}^{-1}$ )	AIP	Air-Inlet-Pressure
$G_m$	Spray mass flow rate ( $\text{kg}\cdot\text{s}^{-1}$ )	WIP	Water-Inlet-Pressure

z	The fitting coefficient	PDWIC	Water-Inlet-Pressure and the Spray Cavity one
Re	Reynolds number	SVFR	Spray Volumetric Flow Rate
We	Weber number	ABAN	Air-Blast Atomization Nozzle
Kn	Knudsen number	SMD	Sauter Mean Diameter
Pr	Prandtl number	GLR	Gas-to-Liquid Ratio
Nu	Nusselt number	APU	Auxiliary Power Unit
x	Parameter substitution symbol	DAS	Data Acquisition Subsystem
<b>Greek symbols</b>			
$\lambda$	Thermal conductivity ( $W \cdot m^{-1} \cdot K^{-1}$ )	TSCS	Tested Spray Cooling Subsystem
$\zeta$	Uncertainty (%)	ASTM	American Society of Testing Materials
$\rho$	Density ( $kg \cdot m^{-3}$ )	TELS	Two-phase Ejector Loop Subsystem
$\sigma$	Surface tension ( $N \cdot m^{-1}$ )	FPCD	Flow and Pressure Control Device
$\kappa$	the mean free path of the molecule	TMS	Thermal Management System
$\mu$	Dynamic viscosity ( $Pa \cdot s$ )	PD	Pressure Difference
$\alpha$	Spray angle ( $^\circ$ )	EP	Environment Pressure
		ABSCS	Air-Blast-Spray-Cooling System
Subscripts		PDWIPSC	Water-Inlet-Pressure and the Spray Cavity one
up	location of up	HX	Heat exchanger

## Appendix A

### Uncertainty Analysis

The maximum uncertainty of the type-K thermocouple is about  $\pm 0.2$  °C, the distance between thermocouples is decided by processing technology, and the geometric manufacturing uncertainty is  $\pm 0.05$  mm. The inlet temperature of water is obtained by PT100 platinum resistor, and the maximum uncertainty is estimated within  $\pm 0.05$  °C in the measuring range of 0–200 °C. Thus, on the basis of the theory of error evaluation as shown in Equation (A1) [37] on this experiment bench, the uncertainty of heat flux, surface temperature and heat transfer coefficient can be expressed as Equations (A2)–(A4).

$$\zeta_y = \pm \sqrt{\sum_{i=1}^n \left( \frac{\partial f}{\partial x_i} \right)^2 \zeta_{x_i}^2} \quad (A1)$$

$$\frac{\partial q}{q} = \sqrt{\left( \frac{\partial \lambda}{\lambda} \right)^2 + \left( \frac{\partial T_{low}}{T_{low}} \right)^2 + \left( \frac{\partial T_{up}}{T_{up}} \right)^2} \quad (A2)$$

$$\frac{\partial T_{sur}}{T_{sur}} = \sqrt{\left( \frac{\partial T_{up}}{T_{up}} \right)^2 + \left( \frac{\partial q}{q} \right)^2 + \left( \frac{\partial l_{s-up}}{l_{s-up}} \right)^2 + \left( \frac{\partial \lambda_{cu}}{\lambda_{cu}} \right)^2} \quad (A3)$$

$$\frac{\partial h}{h} = \sqrt{\left( \frac{\partial q}{q} \right)^2 + \left( \frac{\partial T_{sur}}{T_{sur}} \right)^2 + \left( \frac{\partial T_{in}}{T_{in}} \right)^2} \quad (A4)$$

The uncertainty of heat flux, surface temperature and heat transfer coefficient are  $\pm 3.4\%$ ,  $\pm 4.6\%$  and  $\pm 5.6\%$  respectively. Uncertainties in the pressure and SVFR measurements are estimated to be  $\pm 2.3\%$  and  $\pm 3.1\%$  respectively.

## References

1. Murshed, S.M.S.; De Castro, C.A.N. A critical review of traditional and emerging techniques and fluids for electronics cooling. *Renew. Sustain. Energy Rev.* **2017**, *78*, 821–833. [CrossRef]
2. Wang, J.X.; Li, Y.Z.; Zhang, Y.; Li, J.X.; Mao, Y.F.; Ning, X.W. A hybrid cooling system combining self-adaptive single-phase mechanically pumped fluid loop and gravity-immune two-phase spray module. *Energy Convers. Manag.* **2018**, *176*, 194–208. [CrossRef]
3. O’Keefe, M.; Bennion, K. A comparison of hybrid electric vehicle power electronics cooling options. In Proceedings of the 2007 IEEE Vehicle Power and Propulsion Conference, Arlington, VA, USA, 9–12 September 2007; IEEE: Piscataway, NJ, USA, 2007; pp. 116–123.

4. Liping, P.; Kun, L.; Qi, G.; Shuxin, L.; Chao, Y. Numerical study of high-overload effect on liquid film of spray cooling. *Appl. Therm. Eng.* **2017**, *127*, 1015–1024. [[CrossRef](#)]
5. Elston, L.J.; Yerkes, K.L.; Thomas, S.K.; McQuillen, J. Cooling performance of a 16-nozzle array in variable gravity. *J. Thermophys. Heat Transf.* **2009**, *23*, 571–581. [[CrossRef](#)]
6. Pais, M.R.; Chow, L.C.; Mahefkey, E.T. Surface roughness and its effects on the heat transfer mechanism in spray cooling. *J. Heat Transf.* **1992**, *114*, 211–219. [[CrossRef](#)]
7. Wang, J.X.; Li, Y.Z.; Li, J.X.; Li, C.; Zhang, Y.; Ning, X.W. A gas-atomized spray cooling system integrated with an ejector loop: Ejector modeling and thermal performance analysis. *Energy Convers. Manag.* **2019**, *180*, 106–118. [[CrossRef](#)]
8. Cheng, W.L.; Zhang, W.W.; Chen, H.; Hu, L. Spray cooling and flash evaporation cooling: The current development and application. *Renew. Sustain. Energy Rev.* **2016**, *55*, 614–628. [[CrossRef](#)]
9. Cader, T.; Westra, L.J.; Eden, R.C. Spray cooling thermal management for increased device reliability. *IEEE Trans. Device Mater. Reliab.* **2005**, *4*, 605–613. [[CrossRef](#)]
10. Bancoff, S.G. Stability and dynamics of thin heated liquid films. *Int. J. Fluid Mech. Res.* **1998**, *25*, 189–201. [[CrossRef](#)]
11. Yang, B.H.; Wang, H.; Zhu, X.; Liao, Q.; Ding, Y.D.; Chen, R. Heat transfer enhancement of spray cooling with ammonia by microcavity surfaces. *Appl. Therm. Eng.* **2013**, *50*, 245–250. [[CrossRef](#)]
12. Lin, L.; Ponnappan, R. Heat transfer characteristics of spray cooling in a closed loop. *Int. J. Heat Mass Transf.* **2003**, *46*, 3737–3746. [[CrossRef](#)]
13. Hsieh, C.C.; Yao, S.C. Evaporative heat transfer characteristics of a water spray on micro-structured silicon surfaces. *Int. J. Heat Mass Transf.* **2006**, *49*, 962–974. [[CrossRef](#)]
14. Ashwood, A.C.; Shedd, T.A. Spray cooling with mixtures of dielectric fluids. In Proceedings of the Twenty-Third Annual IEEE Semiconductor Thermal Measurement and Management Symposium, San Jose, CA, USA, 18–22 March 2007; IEEE: Piscataway, NJ, USA, 2007; pp. 144–148.
15. Silk, E.A.; Kim, J.; Kiger, K. Spray cooling of enhanced surfaces: Impact of structured surface geometry and spray axis inclination. *Int. J. Heat Mass Transf.* **2006**, *49*, 4910–4920. [[CrossRef](#)]
16. Monde, M. Critical heat flux in the saturated forced convection boiling on a heated disk with impinging droplets. *Trans. JSME* **1979**, *8*, 54–64.
17. Wang, J.X.; Li, Y.Z.; Li, G.C.; Xiong, K.; Ning, X. Investigation of a gravity-immune chip-level spray cooling for thermal protection of laser-based wireless power transmission system. *Int. J. Heat Mass Transf.* **2017**, *114*, 715–726. [[CrossRef](#)]
18. Pavlova, A.A.; Otani, K.; Amitay, M. Active performance enhancement of spray cooling. *Int. J. Heat Fluid Flow* **2008**, *29*, 262–277. [[CrossRef](#)]
19. Hsieh, S.S.; Fan, T.C.; Tsai, H.H. Spray cooling characteristics of water and R-134a. Part II: Transient cooling. *Int. J. Heat Mass Transf.* **2004**, *47*, 5713–5724. [[CrossRef](#)]
20. Zhou, N.; Chen, F.; Cao, Y.; Chen, M.; Wang, Y. Experimental investigation on the performance of a water spray cooling system. *Appl. Therm. Eng.* **2017**, *112*, 1117–1128. [[CrossRef](#)]
21. Mudawar, I.; Estes, K.A. Optimizing and predicting CHF in spray cooling of a square surface. *J. Heat Transf.* **1996**, *118*, 672–679. [[CrossRef](#)]
22. Navedo, J.E. Parametric Effects of Spray Characteristics on Spray Cooling Heat Transfer. Ph.D. Thesis, University of Central Florida, Orlando, FL, USA, 2001; p. 3809.
23. Yoshida, K.I.; Abe, Y.; Oka, T.; Mori, Y.H.; Nagashima, A. Spray cooling under reduced gravity condition. *J. Heat Transf.* **2001**, *123*, 309–318. [[CrossRef](#)]
24. Silk, E.A.; Kim, J.; Kiger, K. Impact of cubic pin finned surface structure geometry upon spray cooling heat transfer. In Proceedings of the ASME 2005 Pacific Rim Technical Conference and Exhibition on Integration and Packaging of MEMS, NEMS, and Electronic Systems collocated with the ASME 2005 Heat Transfer Summer Conference, San Francisco, CA, USA, 17–22 July 2005; American Society of Mechanical Engineers Digital Collection: New York, NY, USA, 2009; pp. 1–9.
25. Silk, E.A. Investigation of Enhanced Surface Spray Cooling. Ph.D. Thesis, University of Maryland, College Park, MD, USA, 2006.
26. Silk, E.A.; Kim, J.; Kiger, K. Enhanced surface spray cooling with embedded and compound extended surface structures. In Proceedings of the 10th Intersociety Conference on Phenomena in Electronics Systems, San Diego, CA, USA, 30 May–2 June 2006; IEEE: Piscataway, NJ, USA, 2006; pp. 215–223.

27. Silk, E.A.; Gollhofer, E.L.; Selvam, R.P. Spray cooling heat transfer: Technology overview and assessment of future challenges for micro-gravity application. *Energy Convers. Manag.* **2008**, *49*, 453–468. [[CrossRef](#)]
28. Visaria, M.; Mudawar, I. Effects of high subcooling on two-phase spray cooling and critical heat flux. *Int. J. Heat Mass Transf.* **2008**, *51*, 5269–5278. [[CrossRef](#)]
29. Tao, Y.; Huai, X.; Wang, L.; Guo, Z. Experimental characterization of heat transfer in non-boiling spray cooling with two nozzles. *Appl. Therm. Eng.* **2011**, *31*, 1790–1797. [[CrossRef](#)]
30. Jedelsky, J.; Jicha, M. Energy conversion in effervescent atomization. In Proceedings of the 12th ICLASS, Heidelberg, Germany, 2–9 September 2012; pp. 1–9.
31. Beck, J.E.; Lefebvre, A.H.; Koblish, T.R. Liquid sheet disintegration by impinging air streams. *At. Sprays* **1991**, *1*, 155–170. [[CrossRef](#)]
32. Bailardi, G.; Negri, M.; Ciezki, H.K. Several aspects of the atomization behavior of various newtonian fluids with a like-on-like impinging jet injector. In Proceedings of the 23rd European Conference on Liquid Atomization and Spray Systems, Brno, Czech Republic, 6–8 September 2010.
33. Wang, J.X.; Li, Y.Z.; Zhang, H.S.; Wang, S.N.; Mao, Y.F.; Zhang, Y.N.; Liang, Y.H. Investigation of a spray cooling system with two nozzles for space application. *Appl. Therm. Eng.* **2015**, *89*, 115–124. [[CrossRef](#)]
34. Avulapati, M.M.; Venkata, R.R. Experimental studies on air-assisted impinging jet atomization. *Int. J. Multiph. Flow* **2013**, *57*, 88–101. [[CrossRef](#)]
35. Fernandes, M.D.; Andrade, S.D.P.; Bistrizki, V.N.; Fonseca, R.M.; Zacarias, L.G.; Gonçalves, H.N.C.; de Castro, A.F.; Domingues, R.Z.; Matencio, T. SOFC-APU systems for aircraft: A review. *Int. J. Hydrog. Energy* **2018**, *43*, 16311–16333. [[CrossRef](#)]
36. Mao, Y.F.; Li, Y.Z.; Wang, J.X.; Xiong, K.; Li, J.X. Cooling Ability/Capacity and Exergy Penalty Analysis of Each Heat Sink of Modern Supersonic Aircraft. *Entropy* **2019**, *21*, 223. [[CrossRef](#)]
37. Bian, J.; Cao, X.W.; Yang, W.; Edem, M.A.; Yin, P.B.; Jiang, W.M. Supersonic liquefaction properties of natural gas in Laval nozzle. *Energy* **2018**, *159*, 706–715. [[CrossRef](#)]
38. Fan, J.; Chen, B.; Wu, L.; Zhang, F.; Lu, X.; Xiang, Y. Evaluation and development of temperature-based empirical models for estimating daily global solar radiation in humid regions. *Energy* **2018**, *144*, 903–914. [[CrossRef](#)]
39. Tang, Y.; Liu, Z.; Shi, C.; Li, Y. A novel steam ejector with pressure regulation to optimize the entrained flow passage for performance improvement in MED-TVC desalination system. *Energy* **2018**, *158*, 305–316. [[CrossRef](#)]
40. Bian, J.; Jiang, W.; Teng, L.; Liu, Y.; Wang, S.; Deng, Z. Structure improvements and numerical simulation of supersonic separators. *Chem. Eng. Process. Process. Intensif.* **2016**, *110*, 214–219. [[CrossRef](#)]
41. Wang, J.X.; Li, Y.Z.; Yu, X.K.; Li, G.C.; Ji, X.Y. Investigation of heat transfer mechanism of low environmental pressure large-space spray cooling for near-space flight systems. *Int. J. Heat Mass Transf.* **2018**, *119*, 496–507. [[CrossRef](#)]
42. Liu, J.; Xue, R.; Chen, L.; Liu, X.; Hou, Y. Influence of chamber pressure on heat transfer characteristics of a closed loop R134-a spray cooling. *Exp. Therm. Fluid Sci.* **2016**, *75*, 89–95. [[CrossRef](#)]

